Nanoscale

Accepted Manuscript

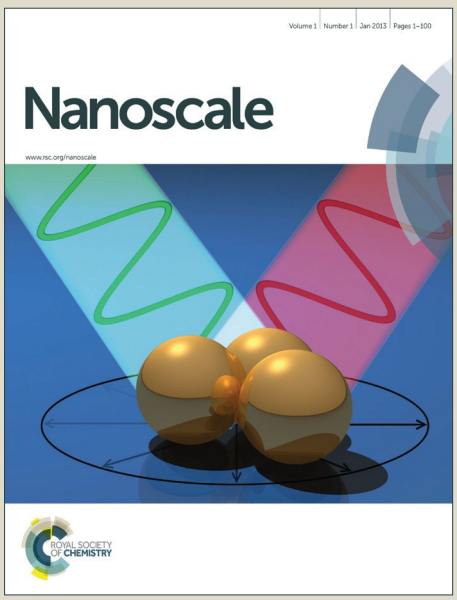

ROYAL SOCIETY OF CHEMISTRY

www.rsc.org/nanoscale

In-situ synthesis of porous array film on filament induced micro-gap electrode pair and their use as resistance-type gas sensor with enhanced performances

Zongke Xu[1], Guotao Duan[1]*, Hongwen Zhang[1], Yingying Wang[1], Lei Xu[2], Weiping Cai[1]*

* Corresponding authors:

duangt@issp.ac.cn (G.D.); wpcai@issp.ac.cn (W.C.);

[1]Key Lab of Materials Physics, Anhui Key Lab of Nanomaterials and Nanotechnology, Institute of Solid State Physics, Chinese Academy of Sciences, Hefei, 230031, PR China

[2]East China Research Institute of Electronic Engineering, 199 Xiangzhang Avenue, Hi-Tech Zone, Hefei, 230088, PR China

Table of Contents

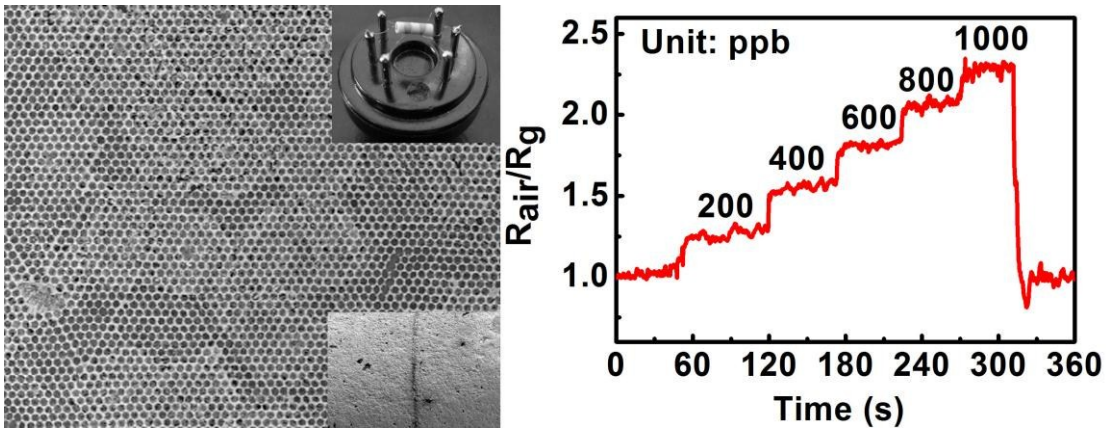

Abstract

The resistance-type metal-oxide semiconductor gas sensors with high sensitivity and low detection limit have been expected for practical applications. It requires both the sensing film with high sensitivity to target gases and the appropriate structure of electrodes-equipped substrate to support sensing films, which still keeps a challenge. In this paper, a new gas sensor of metal-oxide porous array film on micro-gap electrode pair is designed and implemented by taking ZnO as a model material. First, a micro-gap electrode pair was constructed by sputtering deposition on a filament template, which was used as the sensor's supporting substrate. Then, the sensing film of ZnO porous periodic array was in-situ synthesized on the supporting substrate by a solution-dipping colloidal lithography strategy. The results demonstrated the validity of the strategy, and the as-designed sensor shows small device-resistance, enhanced sensing performance with high resolution and ultralow detection limit. This work provides an alternative method to promote the practical application of resistance-type gas sensors.

KEYWORDS: Gas sensor, Colloidal monolayer, Micro-gap electrode pair, Detection limit

Introduction

The resistance-type metal-oxide semiconductor (MOS) gas sensors have attracted great attention in the past few years since the discovery that the adsorption and desorption of gases causes a change in the electrical conductivity of semiconductors.[1-3] Since the first time with the advent of gas sensing element by Taguchi,[4] an enormous amount of efforts have been devoted to gas sensing materials in order to obtain high performances, such as fast response,[5, 6] high sensitivity,[7, 8] low power consumption,[9, 10] low detection limit,[11-13] preferable stability and good selectivity[14, 15]. The emergence of nanomaterials, such as nanoparticles,[16, 17], nanotubes,[18, 19] nanowires,[20-22] nanorods,[23, 24] nanofiber,[25] and hollow spheres,[26-28] leads to enhanced gas performances compared with the bulk materials. In general, these nanostructured sensing films are fabricated on sensor substrates via drop-casting or brush coating. Based on these methods, it is difficult to realize uniformity in film thickness and reproducibility in fabrication. Recently, porous array was fabricated based on colloidal monolayer and used as gas sensing film, which is of patterned pore array and nanosized shells. Gas sensors based such films can solve above problems to a large extent, leading both high sensitivity and nice reproducibility.[29-32]

However, besides the MOS sensing films with excellent performances such as high sensitivity to target gases, the structure of electrodes-equipped device substrate to support sensing films is another important factor to control gas performances, which affects the resistance of gas sensor to a large extent. Usually, smaller the device's resistance, lower the detection limit of gas sensor.[33, 34] Nowadays, there are

mainly two types of sensor substrates including cylindrical and planar sensing-film layouts represented by MEMS-based substrate.[35] Despite of the remarkable characteristics such as portability and flexibility of the planar sensing-film layouts, it is essential to equip with complicated and expensive laboratory apparatus. Therefore, it still remains a great challenge to design a type of gas sensor with a simple device substrate combined highly active sensing thin film.

In this paper, a new gas sensor, i.e. metal-oxide porous array film on micro-gap electrode pair is designed and implemented by taking ZnO as a model material. Other sensors such as Fe_2O_3 and SnO_2 can also be prepared through the same fabrication process only with the change of precursor solution. First, a micro-gap electrode pair was constructed by sputtering deposition on a filament template, which was used as the sensor's supporting substrate. Then, the sensing film of ZnO porous array was in-situ synthesized on the supporting substrate by a solution-dipping colloidal lithography strategy. It was found that the sensor exhibit enhanced sensing performances with lower detection limit and high resolution. This work provides an alternative method to promote the practical applications of MOS gas sensors.

Experimental section

2.1 Preparation

Fabrication of micro-gap electrode pair on device substrate: First, Al_2O_3 ceramic tubes were washed with acetone, ethanol, and distilled water in an ultrasonic bath for 15 min, respectively and then dried in an oven. There is a pair of gold electrodes at each end of the Al_2O_3 ceramic tube, and each electrode was connected

with a pair of Pt wires. The alumina tube was about 4 mm in length, 1.2 mm in external diameter, and 0.8 mm in internal diameter. Second, a filament with the diameter of ca. 20 μm was tied around the ceramic tube. Third, a layer of Ti is coated on the tube's surface by sputtering deposition on Sputter Coater, followed by similar coating of another layer of Au. The sputtering current and time were 20 mA and 1 min, respectively. Lastly, the filament was eliminated from the tube, leaving a micro-gap with several micrometers. Then the micro-gap electrode pair on Al_2O_3 ceramic tube was obtained, which would be used as supporting substrate for the following growth of porous array film.

Growth of ZnO porous array film on micro-gap electrode pair based Al_2O_3 ceramic tube: ZnO porous array film was in-situ synthesized on the supporting substrate by a solution-dipping colloidal lithography strategy. First, ordinary glass slides were washed with acetone, ethanol, and distilled water in an ultrasonic bath and then in turn cleaned in 98% H_2SO_4/H_2O_2 (3:1 in volume), $H_2O/NH_3 \cdot H_2O/H_2O_2$ (5:1:1 in volume), and distilled water, respectively.[36, 37] A suspension of monodispersed polystyrene (PS) spheres with the diameter of 1 μm (2.5 wt% in water, surfactant-free) was obtained from Alfa Aesar. Then, the PS colloidal monolayer template was prepared on the well-cleaned glass slide by air/water interfacial assembly, as is reported.[38-40] A $Zn(NO_3)_2$ aqueous solution (0.1 M) was used as the precursor solution. Based on the route of solution-dipping and transferring the template shown in Figure 1, the PS monolayer floating on the solution surface was picked up with the desired ceramic tube from the solution, and placed flat for 10 min and then dried at 110 ^oC for

10 min in an oven. Finally, the dried substrate covered with the PS colloidal monolayer was annealed at 400 ^{o}C for 2 h to burn the PS spheres away and form ZnO thin films. As a contrast, ZnO porous array film-based sensor on common Al_2O_3 ceramic tube without micro-gap electrode was also fabricated, and we called it "normal sensor" in the following section. The detailed fabrication procedure of ZnO sensing films of normal sensor was the same as that for micro-gap electrode pair based sensor. Similarly, other MOS sensors such as Fe_2O_3 and SnO_2 can be prepared with same method while using different precursor (0.1 M $Fe(NO_3)_3$ for Fe_2O_3 and 0.1 M $SnCl_4$ for SnO_2).

2.2 Characterization and gas sensing measurements

Phase formation of the porous array film was carried out on a Philips X'Pert powder X-ray diffractometer using Cu Ka (0.15419 nm) radiation. The microstructures and morphologies of micro-gap electrode pair and porous array film were characterized by using field-emission scanning electron microscope (FESEM, Sirion200). The gas sensing experiments were carried out in a home-built static testing system with a multimeter/DC power supply (Agilent models U3606 A and U8002A). Two small mixing fans were mounted in the sample chamber to ensure uniform distribution of the target gases in a cuboid chamber with the size of 30 cm x 30 cm x 20 cm in a short time. A certain amount of ethanol-saturated and acetone-saturated vapor was injected into the gas-chamber with sample in the system. The ethanol concentration in the chamber can be calculated on the basis of the injected amount. The measuring electric circuit is shown in Figure S1. These two

types of measuring electric circuits are commonly used in gas sensing measurements. The sensing response was obtained by measuring the change of the electrical voltage of the sensor. The heating voltage (V_h) was supplied to the Ni–Cr alloy coil for heating the sensors, and the circuit voltage (V_c) (Set at 10 V) was supplied across the sensors and the load resistor (R_L), which were connected in series. The output voltage (V_{out}) was the terminal voltage of the load resistor (R_L), which changed depending on the types and concentrations of the gases. The resistance of a sensor in air (R_{air}) or test gas (R_g) was measured by monitoring V_{out}. The relative humidity and temperature in the cuboid chamber was 40% RH and 25 ^oC.

Results and discussion

Based on fabrication routes shown in Figure 1, the porous array film based sensor on micro-gap electrode pair was then prepared. Figure 2a shows the Al_2O_3 ceramic tube coiled by the filament. It can be seen that the diameter of the filament is ca. 18 μm. When the filament is removed, a micro-gap with the width of about 15 μm is left (See Figure 2b). The supporting substrate with the structure of micro-gap electrode pair was thus obtained. The PS colloidal monolayer was prepared in advance based on the air/water interfacial assembly.[38-40] Figure S2a presents a photograph of the PS colloidal monolayer template on the glass slide. It shows iridescent color because of the diffraction effect, indicating the formation of a periodic array structure. The typical corresponding FESEM observation of the PS colloidal monolayer template is shown in Figure S2b. The PS spheres with the diameter of 1 μm are hexagonally close-packed with each other, forming a 2D

colloidal crystal. Then, the PS colloidal monolayer was picked up using the micro-gap electrode pair based ceramic tube after it lifted off the slide and floated on surface of the precursor solution (0.1 M $Zn(NO_3)_2$). From Figure 2c, the PS colloidal monolayer template has been successfully transferred onto the surface of ceramic tube, showing some wrinkles due to the fluctuation of ceramic tube surface. However, the hexagonally arrangements were still retained. Finally, the film was formed after annealing at a high temperature. The sensor was thus obtained, as is shown in the inset in the top right corner of Figure 2d. It consists of the sensing materials, electrodes and the heater. We can see apparently from Figure 2d that the film is of hexagonally arranged porous array structure. Because of some fluctuations of the substrate, the film showed some wrinkles on the ceramic tube (see the inset in the bottom left corner of Figure 2d). Figure S3 shows the X-ray diffraction pattern of the array film. All the peaks are well-matched with the standard PDF card of ZnO (No. 79-0207), indicating a hexagonal wurtzite phase.[30]

Because it is difficult to observe the cross-section image of the ZnO film on the ceramic tube, the sample on the silicon substrate was prepared for exploring the microstructure of the porous array. Figure S4 shows its typical high-magnification FESEM images. It can be seen the total thickness of Ti and Au film is 60 nm (about 30 nm for Ti layer and 30 nm for Au layer), and the thicknesses of porous array film and the pore wall are about 420 nm and 70 nm, respectively. In addition, the periodicity of the array is 1μm.

The ethanol vapor and acetone vapor are chosen as the target gases to study the

gas performances of the ZnO porous array film based sensor on micro-gap electrode pair. Figure S5 shows the response (R_{air}/R_g) of the micro-gap electrode pair based sensor to 10 ppm ethanol at operating temperatures from 150 to 350 ℃, where R_{air} and R_g are the resistances of the sensor before and after exposure to the target gases, respectively. Besides, the sensor signal S is defined as R_{air}/R_{g0} where R_{g0} is the stable or minimal resistance after exposure to the target gas. From Figure S5 we can see that the response of the micro-gap electrode pair based sensor exhibits an optimized response at 300 ^{o}C. In the following experiments, the operating temperatures of all the gas sensing measurements were maintained at 300 ^{o}C. Figure 3a and 3c depicts the electrical resistance of micro-gap electrode pair based sensor and the normal sensor to different concentration of ethanol vapor, respectively. It is noted that the resistance of the normal sensor in the air falls in the level of GΩ. In contrast, the resistance of micro-gap electrode pair based sensor in the air is about 35 MΩ, much smaller than that of the normal sensor. As is known, the smaller resistance can provide stable baseline stability and slight fluctuation for gas sensors under operative mode[33, 42], which is very important to control baseline drift for gas sensors in practical application. The response versus time curves for the normal sensor and micro-gap electrode pair based sensor are shown in Figure 3b and 3d, respectively. It is noted that micro-gap electrode pair based sensor shows a notable on-off behavior with shorter response and recovery time to ethanol vapor, while the normal sensor exhibits longer response and recovery time under the same conditions. In order to study the resolution of these two sensors, a continuous gas sensing measurement without

recoveries was taken in a low concentration range from 1 to 5 ppm as shown in Figure 4. It is observed from Figure 4a and 4b that the normal sensor can still detect ethanol vapor qualitatively with a very poor resolution. However, the electrical response of micro-gap electrode pair based sensor was quite discernible and the ethanol vapor concentration can be accurately quantified (See Figure 4c and 4d), showing a high resolution. Obviously, the higher resolution will bring quantitative detection of target gas, which is very important in applications.

To further study the detection limit of micro-gap electrode pair based sensor, another continuous test without recoveries was performed in a lower concentration range from 200 ppb to 1000 ppb. Figure 5 shows the sensing results when exposed to sub-ppm concentration of ethanol vapor. The incremental change with 200 ppb ethanol vapor could result in a detectable decrease in the resistance, indicating a good ability to detect trace target gas. In this condition, the sensing signal to 200 ppb ethanol is 1.2. However, the normal sensor cannot distinguish the minor change in ethanol vapor concentration. Furthermore, Figure 6 shows sensing response of micro-gap electrode pair based sensor to ethanol vapor at different concentration. The dependence of the sensing signal on the concentration of the target gases can be well described by the empirical equation from MOS gas sensors[44, 45]

$$S=1+AC^{\beta} \qquad (1)$$

Where A is the constant, C the concentration of the target gas with the unit of ppm. The power exponent β, the rational fraction value (usually 1 or 1/2), is related to the charge of the surface species and the stoichiometry of the elementary reactions on the

surface. The inset of Figure 6 represents a linear relation between sensing signal and low concentration of ethanol vapor in the sub-ppm range. To predict the potential detection limit of the micro-gap electrode pair based sensor, a linear dependence in the sub-ppm range is given (Eqn.2),

$$S=1+1.325\times C \qquad (2)$$

In contrast with the normal sensor, the micro-gap electrode pair based sensor displays a strong resolving power to low-concentration ethanol vapor, owing to the low noise in the testing process. Herein, the detection limit is estimated in accordance with the average signal-to-noise ratio. The noise signal σ is observed to be about 0.03 in scale and the standard requirement of the detection limit is (S-1)/ σ>3.[44,45] Therefore, the value of the sensing signal must be larger than 1.03. According to Eqn. (2), the detectable lower limit of concentration to ethanol vapor of micro-gap electrode pair based sensor is about 60 ppb. It should be mentioned that this detection limit is quite low compared with the normal sensor without micro-gap electrode pair, indicating the enhancement in sensing performances by this structure of micro-gap electrode pair. Moreover, this detection limit is much lower compared with the recently reported results in literatures, such as 10 ppm on rhombus-shaped ZnO rod arrays based sensor.[46] In addition, this detectable limit even gets close to the micro-electro-mechanical systems (MEMS)-based sensor.[44] However, the construction of such micro-gap electrode pair based sensor demands less manipulation and it is a general and alternative method for the fabrication of high-performance resistance-type gas sensors.

Besides the measurement to ethanol vapor, acetone vapor is also chosen as the target gas to prove universality of the sensor based on micro-gap electrode pair, as is shown in Figure 7. When exposed to large concentration of acetone vapor, it is noted that micro-gap electrode pair based sensor shows a notable on-off behavior with shorter response and recovery time, while the normal sensor exhibits longer response and recovery time. Besides, the micro-gap electrode pair based sensor exhibits enhanced gas response than the normal sensor. In order to prove the lower detection limit of micro-gap electrode pair based sensor, an amount of acetone vapor with 500 ppb was injected at a time without recovery. (As is shown in Figure 7b) It is obvious that micro-gap electrode pair based sensor can determine acetone vapor as low as 500 ppb, while the normal sensor cannot detect acetone vapor at such low concentration.

Figure 8 plots the sensing responses of the micro-gap electrode pair based sensor for 10 gas-on/off circles to 10 ppm ethanol and acetone vapor at the operating temperature of 300 ℃. The micro-gap electrode pair based sensor exhibits good reproducibility to ethanol and acetone vapor. Figure 9 shows the stability of the micro-gap electrode pair based sensor to 10 ppm ethanol at 300 ^{o}C over 16 months. It should be pointed out that the sensors are not continuously operating at 300 ℃ in 16 mouths. The sensors are kept at room temperature in the rest of the time. Though the response to 10 ppm ethanol decreased slightly as time goes on, the micro-gap electrode pair based sensor largely remains its initial response value, indicating the good stability of the sensors even after 16 months storage.

The gas performances of micro-gap electrode pair based sensor are improved

greatly compared with the normal one. The enhanced gas performances may be attributed to two reasons. First, micro-gap electrode pair leads to a smaller resistance of sensing film, which will bring a lower system noise.[47] Second, micro-gap structure consists of smaller sensing area. Since it is impossible that the sensing properties in different positions of the film are identical, the smaller area can easily lead to the similar properties, which may be advantageous to obtain both a response with slighter fluctuation and a smaller noise.

As is known, the porous array film based sensor displays high sensitivity and stability while it is not easy to achieve a low detection limit owing to the large resistance of this film structure. However, the use of micro-gap electrode pair could lead to a very low detection limit and a high resolution. More importantly, this sensor structure and construction method can also be applied to other sensing materials by changing the precursor solution, such as Fe_2O_3, SnO_2. X-ray diffraction patterns in Figure S6 demonstrate the formation of SnO_2 and Fe_2O_3. Both the sensing films consist of porous periodic array structure, showing a little difference owing to different metal oxides. As is shown in Figure S7, Fe_2O_3 and SnO_2 micro-gap electrode pair based sensors also show similar enhancement effect, with higher resolution to ethanol vapor.

Conclusion

In summary, a new MOS gas sensor of metal-oxide porous array film on micro-gap electrode pair is designed and constructed by taking ZnO as a model material. Such micro-gap electrode pair based sensor exhibits enhanced gas

performances to ethanol and acetone vapor with higher resolution and lower detection limit owing to a smaller resistance than the normal sensor. This strategy will allow researchers and manufacturers to produce low-cost sensors with high gas performances through a simplified process.

Acknowledgements

The authors acknowledge the national basic research program of China (973 Program, Grant No. 2011CB302103), the financial supports from natural science foundation of China (Grant No. 51471161, 11174286, 11374303, 11404337 and 61306143), and Anhui provincial natural science foundation for distinguished young scholar (1408085J10).

Figure captions

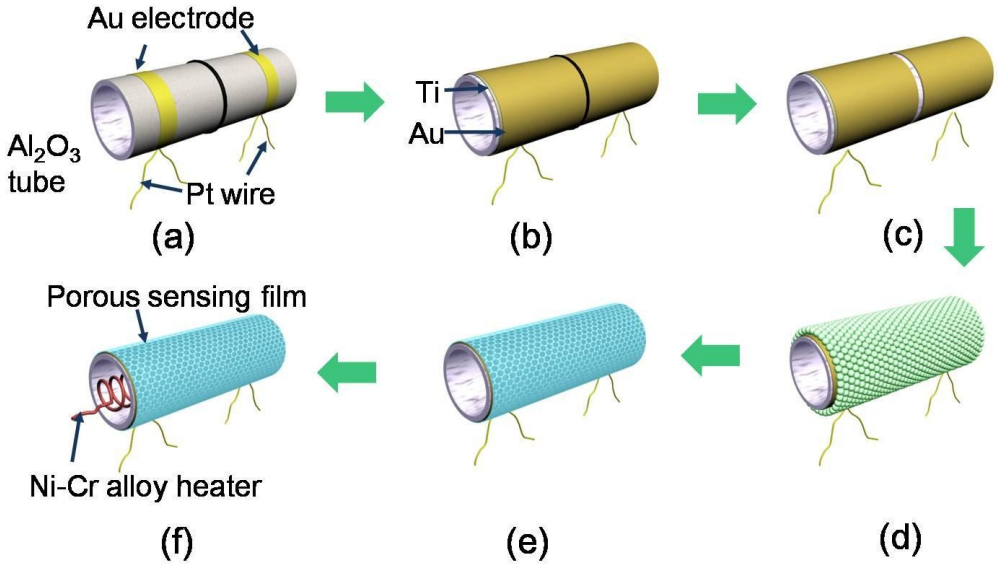

Figure 1. Schematic illustration of the fabrication routes for micro-gap electrode pair based sensor. (a): A filament with the diameter of ca. 20 μm is tied around the Al_2O_3 ceramic tube. (b) Ti and Au layer are coated on the tube's surface by sputtering deposition, respectively. (c) The filament is eliminated from the tube, leaving a micro-gap on ceramic tube. (d) $Zn(NO_3)_2$ solution dipped PS colloidal monolayer was transferred onto the micro-gap electrode pair based ceramic tube. (e) ZnO porous array film is formed after annealing at a high temperature. (f) The Ni-Cr heater is embedded in the ceramic tube as a heating electrode, and the sensor was thus obtained.

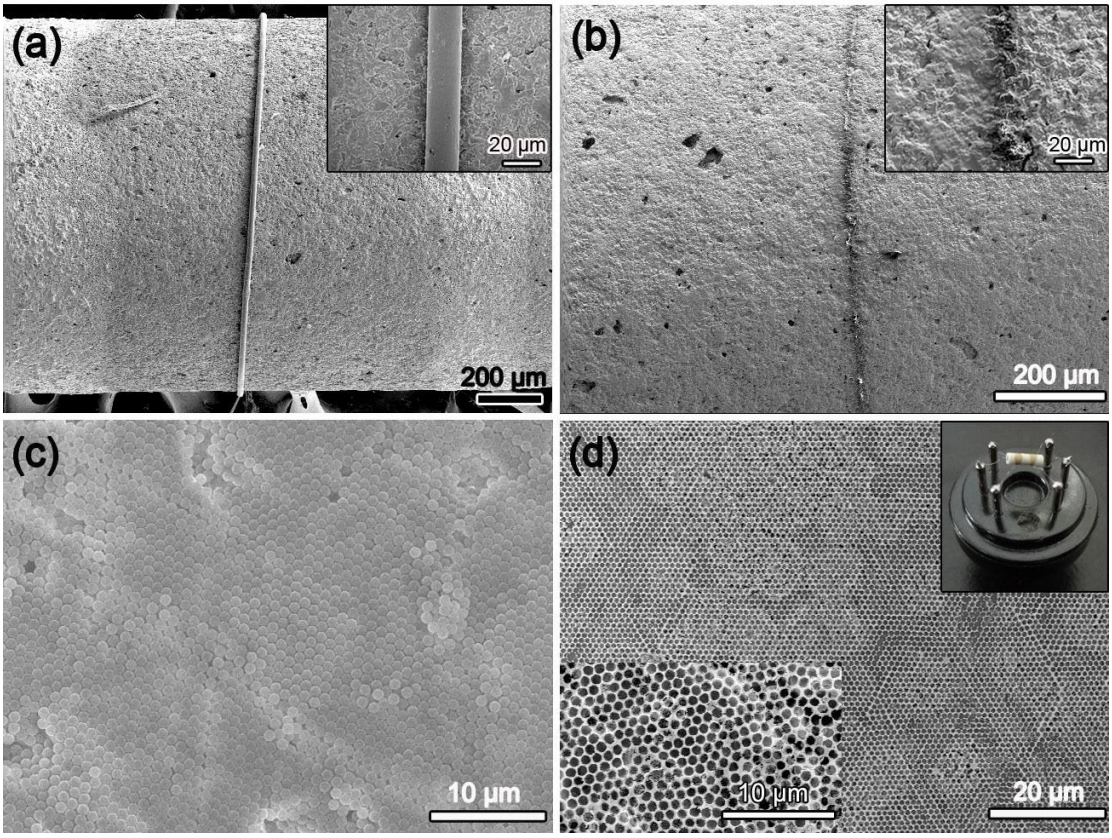

Figure 2. (a) The FESEM image of Al_2O_3 ceramic tube coiled by a filament. The inset is a magnified FESEM image. (b) The FESEM image of Al_2O_3 ceramic tube after the elimination of the filament. The inset is the magnified FESEM image. (c) The FESEM image of the transferred PS colloidal monolayer template on the Al_2O_3 ceramic tube after solution dipping in $Zn(NO_3)_3$ solution. (d) The typical FESEM image of ZnO porous array films on the Al_2O_3 ceramic tube. The inset at the top right corner is the physical map of the as-prepared sensor.

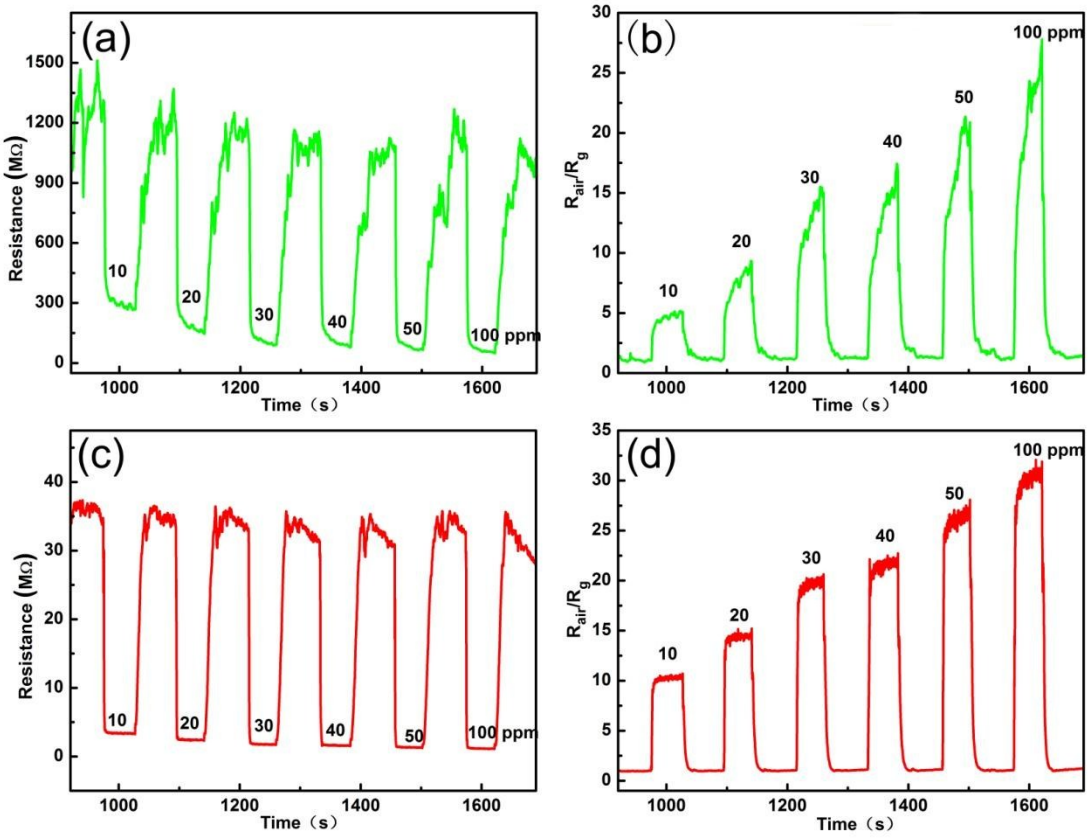

Figure 3. (a) Resistance change and (b) response of ZnO porous array film based on the Al_2O_3 ceramic tube without micro-gap electrode pair to ethanol vapor. (c) Resistance change and (d) response of ZnO porous array film based on the Al_2O_3 ceramic tube with micro-gap electrode pair to ethanol vapor.

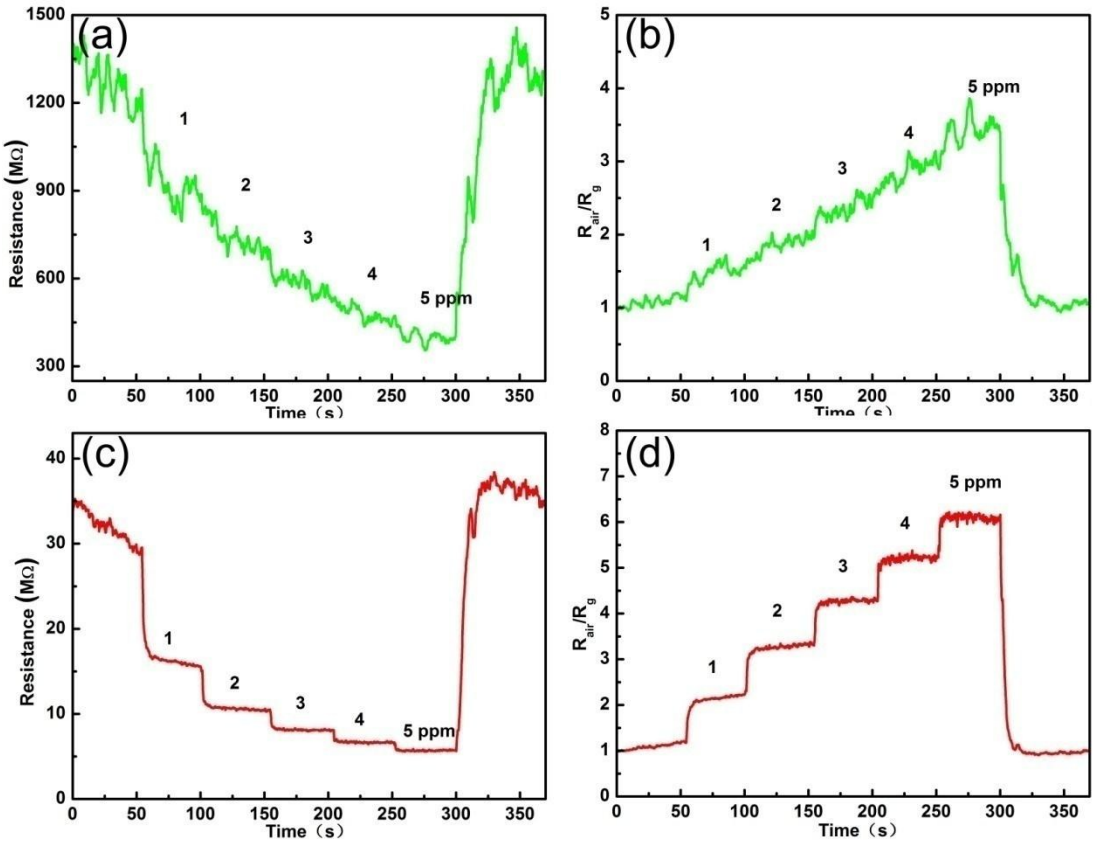

Figure 4. A continuous gas sensing measurement without recovery to 1-5 ppm ethanol vapor. (a) Resistance change and (b) response for the normal sensor. (c) Resistance change and (d) response for the micro-gap electrode pair based sensor.

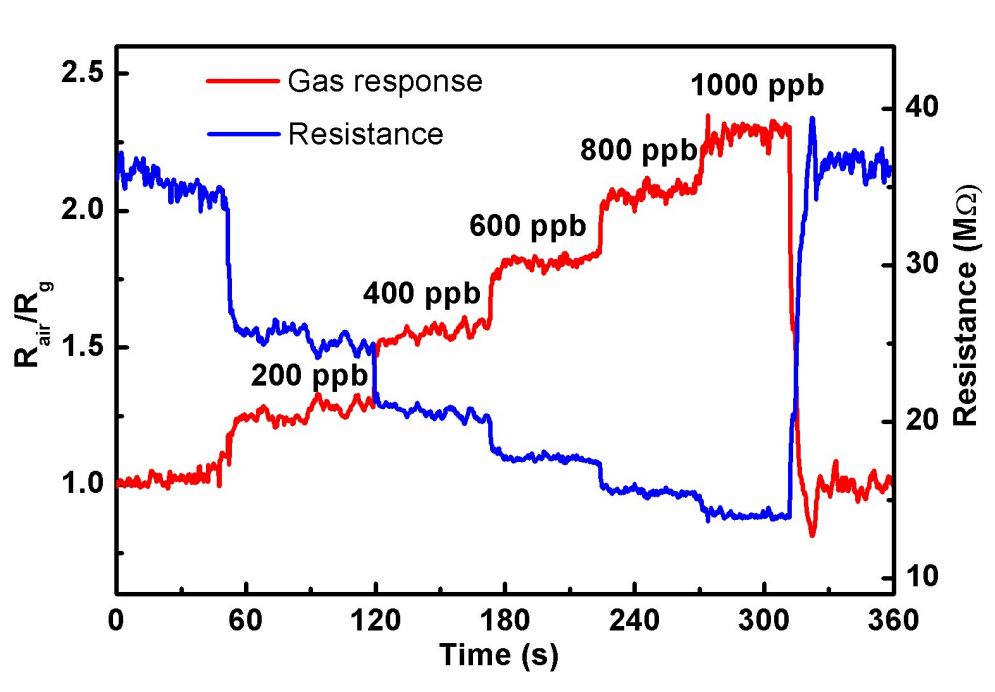

Figure 5. A continuous gas sensing measurement for micro-gap electrode pair based sensor without recoveries to 200-1000 ppb ethanol vapor.

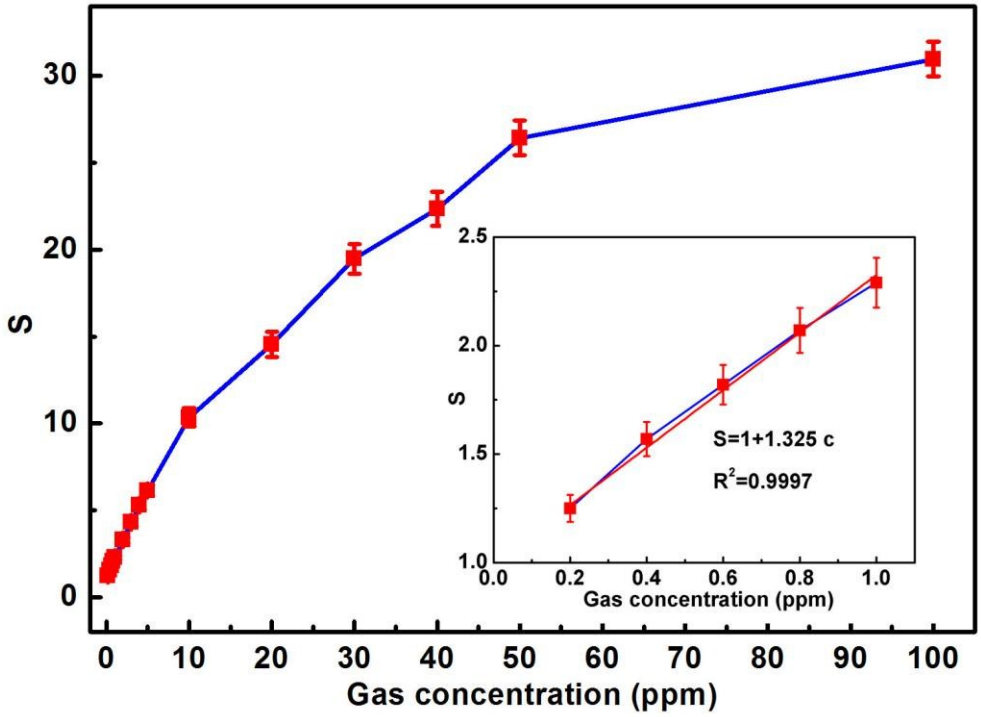

Figure 6. The sensing response (s) vs. ethanol vapor concentration for micro-gap electrode pair based sensor. The inset is the corresponding sensing response (s) vs. gas concentration linear fitting curve.

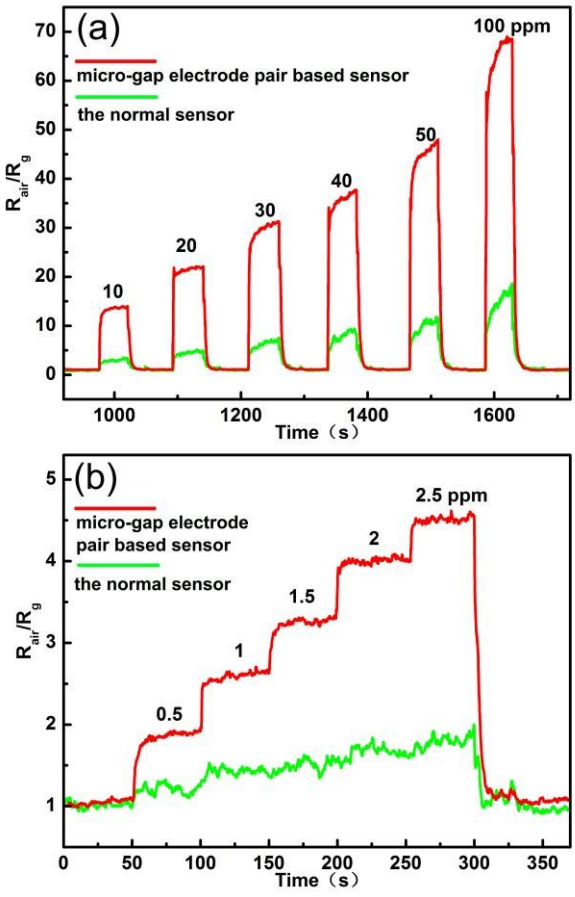

Figure 7. Sensing response vs. different concentration of acetone vapor. The red and green curve represent the micro-gap electrode pair based sensor and the normal sensor respectively.

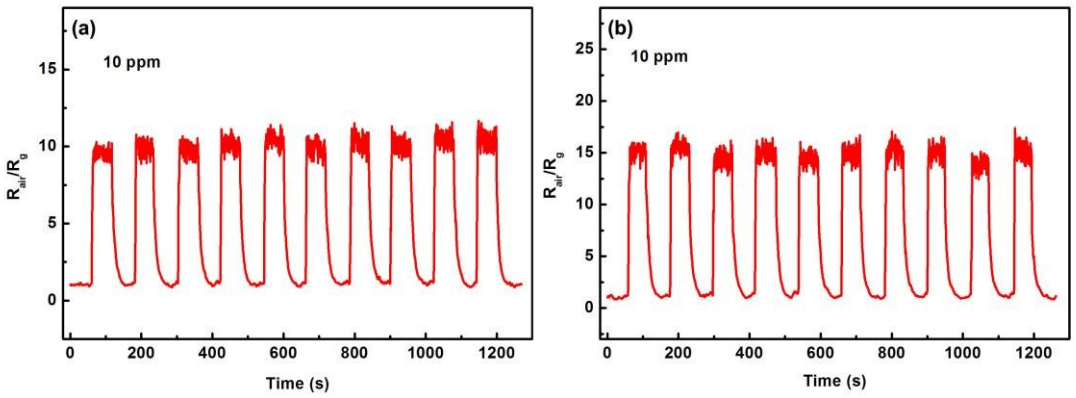

Figure 8. Sensing responses of the micro-gap electrode pair based sensor for 10 gas-on/off circles to 10 ppm (a) ethanol and (b) acetone vapor.

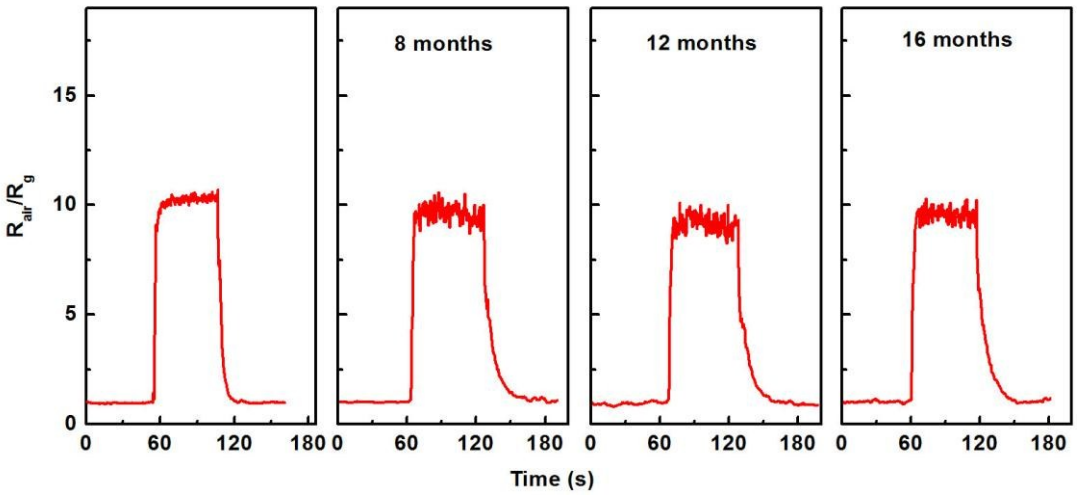

Figure 9. The stability of sensing response to 10 ppm ethanol vapor over 16 months.

Reference

1 A. Gurlo, *Nanoscale*, 2011, **3**, 154-165.

2 G. Korotcenkov and B. K. Cho, *Crit. Rev. Solid State*, 2010, **35**, 1-37.

3 S. J. Pearton, F. Ren, Y.-L. Wang, B. H. Chu, K. H. Chen, C. Y. Chang, W. Lim, J. Lin and D. P. Norton, *Prog. Mater. Sci.*, 2010, **55**, 1-59.

4 T. Naoyoshi, Google Patents, 1972.

5 P. Sowti khiabani, E. Marzbanrad, H. Hassani, B. Raissi and S. Bhandarkar, *J. Am. Ceram. Soc.*, 2013, **96**, 2493-2498.

6 S. Wang, Y. Xiao, D. Shi, H. K. Liu and S. X. Dou, *Mater. Chem. Phys.*, 2011, **130**, 1325-1328.

7 D.-J. Yang, I. Kamienchick, D. Y. Youn, A. Rothschild and I.-D. Kim, *Adv. Funct. Mater.*, 2010, **20**, 4258-4264.

8 Y. Zhang, J. Xu, P. Xu, Y. Zhu, X. Chen and W. Yu, *Nanotechnology*, 2010, **21**, 288501-288508.

9 C. Hagleitner, A. Hierlemann, D. Lange, A. Kummer, N. Kerness, O. Brand and H. Baltes, *Nature*, 2001, **414**, 293-296.

10 E. N. Dattoli, A. V. Davydov and K. D. Benkstein, *Nanoscale*, 2012, **4**, 1760-1769.

11 L. Senesac and T. G. Thundat, *Mater. Today*, 2008, **11**, 28-36.

12 M. Xue, F. Li, Y. Wang, X. Cai, F. Pan and J. Chen, *Nanoscale*, 2013, **5**, 1803-1805.

13 J. Ma, L. Mei, Y. Chen, Q. Li, T. Wang, Z. Xu, X. Duan and W. Zheng, *Nanoscale*, 2013, **5**, 895-898.

14 L. Yin, D. Chen, X. Cui, L. Ge, J. Yang, L. Yu, B. Zhang, R. Zhang and G. Shao, *Nanoscale*, 2014, **6**, 13690-13700.

15 N. Gaikwad, S. Bhanoth, P. V. More, G. H. Jain and P. K. Khanna, *Nanoscale*, 2014, **6**, 2746-2751.

16 N. G. Cho, I.-S. Hwang, H.-G. Kim, J.-H. Lee and I.-D. Kim, *Sens. Actuators, B*, 2011, **155**, 366-371.

17 E. R. Leite, I. T. Weber, E. Longo and J. A. Varela, *Adv. Mater.*, 2000, **12**, 965-968.

18 N. Du, H. Zhang, B. D. Chen, X. Y. Ma, Z. H. Liu, J. B. Wu and D. R. Yang, *Adv. Mater.*, 2007, **19**, 1641-1645.

19 J. Chen, L. Xu and W. Ii, *Adv. Mater.*, 2005, **17,** 582-586.

20 H. W. Ra, K. S. Choi, J. H. Kim, Y. B. Hahn and Y. H. Im, *Small*, 2008, **4**, 1105-1109.

21 F. Yang, D. K. Taggart and R. M. Penner, *Small*, 2010, **6**, 1422-1429.

22 M. C. McAlpine, H. Ahmad, D. Wang and J. R. Heath, *Nat. Mater.*, 2007, **6**, 379-384.

23 L. Shi, A. J. Naik, J. B. Goodall, C. Tighe, R. Gruar, R. Binions, I. Parkin and J. Darr, *Langmuir*, 2013, **29**, 10603-10609.

24 H. Huang, H. Gong, C. L. Chow, J. Guo, T. J. White, M. S. Tse and O. K. Tan, *Adv. Funct. Mater.*, 2011, **21**, 2680-2686.

25 S. Bai, S. Chen, Y. Zhao, T. Guo, R. Luo, D. Li and A. Chen, *J. Mater. Chem. A*, 2014, **2**, 16697-16706.

26 B. Li, Y. Xie, M. Jing, G. Rong, Y. Tang and G. Zhang, *Langmuir*, 2006, **22**, 9380-9385.

27 G. Liu, W. Cai, L. Kong, G. Duan, Y. Li, J. Wang and Z. Cheng, *J. Hazard. Mater.*, 2013, **248-249**, 435-441.

28 P. Sun, X. Zhou, C. Wang, K. Shimanoe, G. Lu and N. Yamazoe, *J. Mater. Chem.*

A, 2014, **2**, 1302-1308.

29 Z. Dai, L. Jia, G. Duan, Y. Li, H. Zhang, J. Wang, J. Hu and W. Cai, *Chem.-Eur. J.*, 2013, **19**, 13387-13395.

30 Z. Xu, G. Duan, Y. Li, G. Liu, H. Zhang, Z. Dai and W. Cai, *Chem.-Eur. J.*, 2014, **20**, 6040-6046.

31L.Li, Y.Li, S. Gao and N. Koshizaki, *J. Mater. Chem.*, 2009, **19**, 8366–8371.

32 L. Jia, W. Cai, H. Wang, F. Sun and Y. Li, *ACS Nano*, 2009, **3**, 2697-2705.

33 G. Jimenez-Cadena, J. Riu and F. X. Rius, *Analyst*, 2007, **132**, 1083-1099.

34 J. Lee, W. Shim, E. Lee, J. S. Noh and W. Lee, *Angew. Chem.,Int. Ed.*, 2011, **50**, 5301-5305.

35 A. Tricoli, M. Righettoni and A. Teleki, *Angew. Chem.,Int. Ed.*, 2010, **49**, 7632-7659.

36 L. Jia and W. Cai, *Adv. Funct. Mater.*, 2010, **20**, 3765-3773.

37 H. Zhang, G. Duan, G. Liu, Y. Li, X. Xu, Z. Dai, J. Wang and W. Cai, *Nanoscale*, 2013, **5**, 2460-2468.

38 Z. Dai, Y. Li, G. Duan, L. Jia and W. Cai, *ACS Nano*, 2012, **6**.

39 J. Wang, G. Duan, G. Liu, Y. Li, Z. Dai, H. Zhang and W. Cai, *J. Mater. Chem.*, 2011, **21**, 8816-8821.

40 L. Li, T. Zhai, H. Zeng, X. Fang, Y. Bando and D. Golberg, *J. Mater. Chem.*, 2011, **21**, 40-56.

41 J. Wang, G. Duan, Y. Li, G. Liu, Z. Dai, H. Zhang and W. Cai, *Langmuir*, 2013, **29**, 3512-3517.

42 M. Huebner, D. Koziej, M. Bauer, N. Barsan, K. Kvashnina, M. D. Rossell, U. Weimar and J.-D. Grunwaldt, *Angew. Chem. Int. Edit.*, 2011, **50**, 2841-2844.

43 I.-D. Kim and A. Rothschild, *Nano Lett.*, 2006, **6,** 193-198.

44 Z. Dai, L. Xu, G. Duan, T. Li, H. Zhang, Y. Li, Y. Wang and W. Cai, *Sci. Rep.*, 2013, **3**, 1669-1676.

45 R. W. J. Scott, S. M. Yang, G. Chabanis, N. Coombs, D. E. Williams and G. A. Ozin, *Adv. Mater.*, 2001, **13**, 1468-1472.

46 Z. Wen, L. Zhu, Z. Zhang and Z. Ye, *Sens. Actuators, B*, 2015, **208**, 112–121.

47 G. Korotcenkov and B. K. Cho, *Sens. Actuators, B*, 2014, **198**, 316-341.